

Tensor network simulation of phase diagram of frustrated J_1 - J_2 Heisenberg model on a checkerboard lattice

Y.-H. Chan^{1,2}, Y.-J. Han^{1,3}, and L.-M. Duan^{1,2}

¹*Department of Physics and MCTP, University of Michigan, Ann Arbor, Michigan 48109, USA*

²*Center for Quantum Information, IIIS, Tsinghua University, Beijing, China and*

³*Key laboratory of Quantum Information, University of Science and Technology of China, Hefei, Anhui 230026, People's Republic of China*

We use the recently developed tensor network algorithm based on infinite projected entangled pair states (iPEPS) to study the phase diagram of frustrated antiferromagnetic J_1 - J_2 Heisenberg model on a checkerboard lattice. The simulation indicates a Neel ordered phase when $J_2 < 0.88J_1$, a plaquette valence bond solid state when $0.88 < J_2/J_1 < 1.11$, and a stripe phase when $J_2 > 1.11J_1$, with two first-order transitions across the phase boundaries. The calculation shows the cross-dimer state proposed before is unlikely to be the ground state of the model, although such a state indeed arises as a metastable state in some parameter region.

PACS numbers:

Understanding frustrated quantum magnetic models is a long standing difficult problem in strongly correlated physics. Theoretical tools to study these systems are limited. Exact diagonalization is limited by the small system size, and quantum Monte-Carlo simulation is hindered by the infamous sign problem. Among the frustrated models, the antiferromagnetic J_1 - J_2 Heisenberg model on a checkerboard lattice (or called the crossed chain model) is an important example that has raised a lot of interest [1–7], due to its rich phase diagram and connection with real materials. This model is described by the Hamiltonian

$$H = J_1 \sum_{\langle i,j \rangle} \vec{S}_i \cdot \vec{S}_j + J_2 \sum_{\langle\langle i,j \rangle\rangle} \vec{S}_i \cdot \vec{S}_j \quad (1)$$

where J_1 is the nearest-neighbor spin coupling rate on a square lattice and J_2 is the next-nearest-neighbor spin coupling rate on a checkerboard pattern of plaquettes, as depicted in Fig. 1. A number of works provide complementary studies in different parameter regions. The complete phase diagram for this model, however, still remains controversial. It is known that the system has a collinear long-range Neel order when $J_2 \ll J_1$. At $J_1 \approx J_2$, the calculation based on the strong-coupling expansion predicts a plaquette valence bond solid as the ground state [1, 3–5]. In the region with $J_2 > J_1 > 0$, the phase is still under debate. Possibilities include the fourfold degenerate state with long range spin order, supported with semi-classical studies [6] and large- N expansion calculation [7], the sliding Luttinger liquid phase, supported with perturbative random phase calculation and exact diagonalization of a small system [1], and the cross dimer state, supported with bosonization approach [3] and two-step DMRG (density-matrix renormalization group) simulation [4].

Recently, tensor network algorithms emerge as a promising method to solve two-dimensional frustrated quantum systems [8–12]. There are different types of

tensor network algorithms, but all the algorithms share the basic idea to describe the ground state of the model Hamiltonian as a tensor network state that respects the entanglement area law. The tensor network algorithms belong to the variational method and have no intrinsic sign problem for frustrated systems. The tensor network algorithms have been tested for a number of non-frustrated Hamiltonians, and the results agree pretty well with quantum Monte Carlo simulation [10]. Recently, the algorithms have also been applied to the frustrated Heisenberg model on a Kagome lattice [11] and the J_1 - J_2 - J_3 model on a square lattice [12].

In this paper, we use a particular type of tensor network algorithm, the iPEPS (infinite PEPS) [9], to simulate frustrated antiferromagnetic J_1 - J_2 model on a checkerboard lattice in the thermodynamic limit. We construct the complete phase diagram with the following findings: (1) the simulation shows two first-order phase transitions respectively at $J_2/J_1 = 0.88$ and $J_2/J_1 = 1.11$, first from a Neel state to a plaquette valence bond solid, and then to a spin ordered stripe phase. (2) In the region with $J_2/J_1 > 1.11$ (except for the special point $J_1 = 0$), our calculation supports the four-fold degenerate states proposed in Ref. [6] as the ground state. In particular, the spin stripe phase seems to be the most stable one under perturbation. (3) Our simulation provides strong evidence to show that the cross-dimer state is not the ground state of the system, although it indeed emerges as a metastable state in some parameter region (its energy is always significantly higher compared with the spin stripe phase).

In the iPEPS algorithm, at every site, we represent the state as a five-index tensor with one physical index (with dimension two for a spin-half system) and four virtual indices (with internal dimension denoted by D) [9]. The wave function can be obtained by contracting all the virtual indices. To obtain the expectation value of a physical quantity, we need to first contract the physical index to

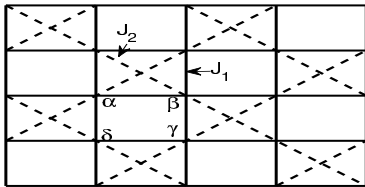


FIG. 1: Illustration of the $J_1 - J_2$ Heisenberg model on a checkerboard lattice.

form a tensor network with internal dimension D^2 , and this tensor network is then contracted from the infinite boundary through multiplication with a matrix product state with internal dimension χ . We tune the value of χ until convergence is achieved in the calculated physical quantity. As a thumb of rule, typically at $\chi \gtrsim D^2$, the relative error of energy induced by variation of χ has been reduced to the order of 10^{-5} , which indicates good convergence already. The dominant error of the calculation is from the small value of the internal dimension D . As the calculation time scales with D as D^{12} (under choice of $\chi \sim D^2$) [9], the value of D in our simulation is limited to be about 5. We compare the energy as well as several other quantities (including the phase boundary specified below in Fig. 2) calculated with $D = 4$ and $D = 5$, and the difference is within a percent level. As an estimate, we expect that the relative error of our numerical simulation, dominated by the limited value of D , is within

$$Q_{\alpha\beta\gamma\delta} = 2 \left[\langle \vec{S}_\alpha \cdot \vec{S}_\beta \rangle \langle \vec{S}_\gamma \cdot \vec{S}_\delta \rangle + \langle \vec{S}_\alpha \cdot \vec{S}_\delta \rangle \langle \vec{S}_\beta \cdot \vec{S}_\gamma \rangle - \langle \vec{S}_\alpha \cdot \vec{S}_\gamma \rangle \langle \vec{S}_\beta \cdot \vec{S}_\delta \rangle \right] + 1/2 \left[\langle \vec{S}_\alpha \cdot \vec{S}_\beta \rangle + \langle \vec{S}_\gamma \cdot \vec{S}_\delta \rangle + \langle \vec{S}_\alpha \cdot \vec{S}_\delta \rangle + \langle \vec{S}_\beta \cdot \vec{S}_\gamma \rangle \langle \vec{S}_\alpha \cdot \vec{S}_\gamma \rangle + \langle \vec{S}_\beta \cdot \vec{S}_\delta \rangle + 1/4 \right], \quad (2)$$

where α , β , γ , and δ denote four spins on a plaquette as shown in Fig. 1. Different phases are associated with different characteristic values of these parameters. For instance, a spin ordered state is characterized by a significant value of $\langle \vec{S}_i \rangle$; in contrast, the plaquette valence bond solid state is characterized by a near-unity $Q_{\alpha\beta\gamma\delta}$ and a vanishing $\langle \vec{S}_i \rangle$.

In the inserts of Fig. 2, we show the order parameters $\langle \vec{S}_i \rangle$ and $Q_{\alpha\beta\gamma\delta}$ as functions of J_2/J_1 . These order parameters change abruptly at the corresponding phase transition points, and the points of abrupt change are in agreement with the singularity points of $\frac{\partial E}{\partial J_2}$. The order parameters and the derivative of the ground state energy both have finite jumps at the phase transition points, which strongly indicates that we have two first-

or about a percent level for any short-range correlation function.

The original iPEPS algorithm needs to assume translational symmetry for calculation in the thermodynamical limit. The ground state of the Hamiltonian (1) can spontaneously break the translational symmetry. To take into account the spontaneous symmetry breaking, we take a large unit cell and assume the translational symmetry only among different cells with no symmetry restriction for the tensors within the cell. In our simulation, the unit cell has 4×4 sites which is large enough to incorporate the relevant ground states for this Hamiltonian that break the translational symmetry [13]. We apply imaginary time evolution to reach the ground state of the Hamiltonian. To avoid being stuck in a metastable state, we take a number of random initial states for the imaginary time evolution and pick up the ground state as the one which has the minimum energy over all the trials.

In Fig. 3, we show the complete phase diagram for the Hamiltonian (1) from this calculation. To characterize the phase transition, we calculate derivative of the ground state energy $\frac{\partial E}{\partial J_2} = \sum_{\langle\langle i,j \rangle\rangle} \langle \vec{S}_i \cdot \vec{S}_j \rangle$ with respect to J_2 (J_1 is taken as the energy unit) and identify the singular point of this derivative as the phase transition point. To characterize properties of different phases, we calculate the spin order parameter $\langle \vec{S}_i \rangle$ for all sites i and the plaquette order parameter $Q_{\alpha\beta\gamma\delta}$ [14], defined by

order transitions as we increase the ratio J_2/J_1 , first from a Neel ordered state to a plaquette valence bond solid state at $J_2/J_1 = 0.88$, and then from the valence bond solid state to another spin-ordered phase (its nature will be discussed below) at $J_2/J_1 = 1.11$. The possibility of two second order phase transitions with a coexistence region of the spin and the valence bond solid orders in the intermediate region has been discussed in the literature [15]. Within the resolution of our numerical simulation (the resolution is 0.01 for the ratio J_2/J_1 near the phase transition points), we do not find a coexistence region and the result supports a direct first-order transition.

The nature of ground states in these three phases are further studied through calculation of the spin correlation function. In Fig. 3, We show the nearest-neighbor spin-spin correlation $\langle \vec{S}_i \cdot \vec{S}_j \rangle$ and orientation of local spins

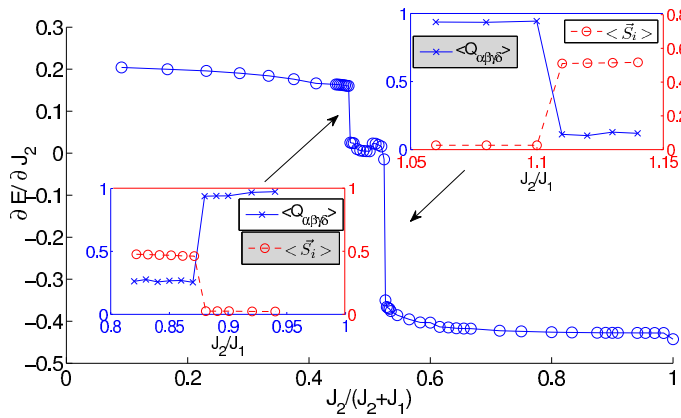


FIG. 2: (Color online) The main plot shows $\partial E/\partial J_2$ as a function of $J_2/(J_1 + J_2)$. Insets show the plaquette order (solid line with crosses) and the spin order (red dashed line with circles) as functions of J_2/J_1 near the transition points.

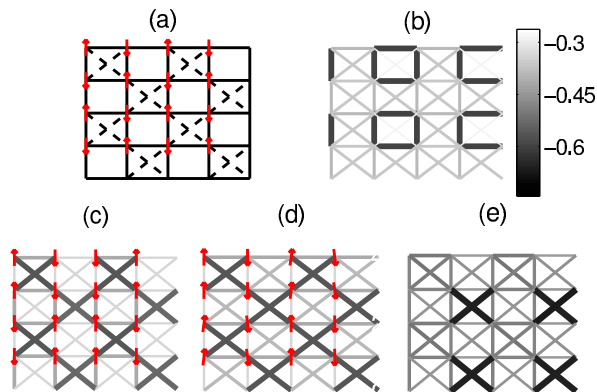


FIG. 3: (Color online) The upper left figure (a) shows orientations of local spins (red arrows) on the checkerboard lattice at $J_2 = 0.5$. The upper right figure (b) shows nearest neighbor spin-spin correlations $\langle \vec{S}_i \cdot \vec{S}_j \rangle$ along horizontal, vertical and diagonal bonds on a 16-site unit-cell at $J_2 = 1.0$. The width and colors of the bonds are scaled such that the negative correlation is represented by thicker bonds with darker color. The lower figures show both spin orientation and correlations $\langle \vec{S}_i \cdot \vec{S}_j \rangle$ in a Neel* state (c) and a stripe phase (d) at $J_2 = 2$. Fig. (e) illustrates the dimer state, which appears as a metastable state at some parameters.

with respect to the first spin on the up-left corner in each 16-site unit-cell for three different J_2 values. At $J_2 = 1$, strong nearest-neighbor spin correlations (valence bonds) around the plaquettes breaking the lattice translational symmetry suggests a plaquette ordered state near this point, consistent with the finding in Fig. 2. At $J_2 = 0.5$, the spin orientation indicates a conventional Neel ordered state. At $J_2 = 2$, antiferromagnetic Neel order appears along the diagonal chains, but not in the horizontal or vertical axes. With imaginary time evolution starting from randomly chosen initial states, we actually get two

different kinds of spin configurations shown in Fig. 3(c) and 3(d) for the final state. Their energies are almost degenerate within resolution of our numerical program. These spin configurations are in agreement with the four-fold degenerate states found in Ref. [6] based on the large- S expansion (the other two degenerate states are obtained from Fig. 3(c) and 3(d) through a 90-degree rotation of the spin orientation). The spin configuration in Fig. 3(c) is called the Neel*-state in Ref. [3], where the single-site spin \uparrow or \downarrow in the conventional Neel state is replaced by the two-site unit $\uparrow\uparrow$ or $\downarrow\downarrow$. The configuration in Fig. 3(d) represents a spin stripe phase, where the spin orientations form a stripe along the horizontal or vertical direction, breaking the lattice rotational symmetry. The stripe phase is also predicted in the large- N calculation [7].

To further clarify the phase at $J_2 = 2$, we also show the spin-spin correlation $\langle \vec{S}_i \cdot \vec{S}_j \rangle$ in Fig. 3(c) and 3(d). Strong nearest-neighbor spin correlation appears along the diagonal chains. However, the distribution of these spin correlations does not break the symmetry of the lattice, so it is not a cross dimer or other valence bond solid state. The cross dimer state is predicted for this model in [3, 4] for some region of J_2/J_1 . In a cross dimer state, the nearest-neighbor spin correlations form the cross dimer pattern illustrated by Fig. 3(e). We indeed get this kind of cross dimer configuration from the imaginary time evolution starting from a pure cross dimer state for a certain region of J_2/J_1 as shown in Fig. 4. However, the energies of the cross dimer states are strictly higher than the four-fold degenerate states shown in Fig. 3(c) and 3(d). So the cross dimer state is only a metastable phase in this region and does not give the real ground state. We compare the energy of our calculation with the energy of the DMRG calculation in Ref. [4], and our energy is significantly lower than the corresponding result in [4] on the side $J_2 > J_1$. For instance, at $J_2 = 2$, our result shows a ground state energy of $E = -0.876J_1$ for a stripe state, much lower than the energy of $E \simeq -0.75J_1$ for a cross dimer state at the corresponding point in Ref. [4]. Because of this large energy difference, it is unlikely that the cross dimer state emerges as the real ground state of the system.

Some literature predicts a sliding Luttinger liquid state on the $J_2 > J_1$ side of the antiferromagnetic checkerboard model [1, 2]. We do not find evidence to support a transition to a sliding Luttinger liquid state in our numerical simulation. Of course, due to the limitation of the internal dimension D of the variational tensor network state in our calculation, it is possible that the sliding Luttinger liquid state is poorly approximated by the tensor network state with a small internal dimension and thus missed in our numerical simulation. We can not rule out this possibility, however, we feel its chance is small due to the following test: we know at the limiting point $J_1 = 0$,

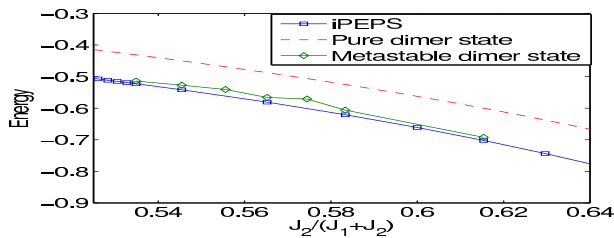


FIG. 4: (Color online) Ground state energy calculated by iPEPS (blue squares) for different $J_2/(J_2 + J_1)$. The dashed line denotes energy of a pure dimer state, the green diamonds denote energy of meta-stable dimer states calculated by iPEPS with imaginary time evolution from an initial pure dimer state.

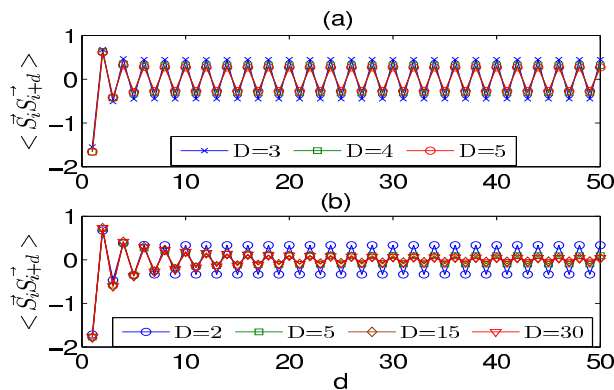


FIG. 5: (Color online) (a) Long-range spin correlations along a diagonal chain obtained with $D = 3$ (crosses), $D = 4$ (squares), and $D = 5$ (circles) at $J_2 = 2$. (b) The same correlation for a Heisenberg chain calculated with $D = 3$ (circles), $D = 5$ (squares), $D = 15$ (diamonds), and $D = 30$ (triangles).

the model reduces to decoupled Heisenberg chains whose ground state is described by a Luttinger liquid with algebraic decay of the spin correlation function. We use the same tensor network algorithm to calculate the long range spin correlation for the limiting case at $J_1 = 0$. At this 1D limiting point, we can have a much larger internal dimension D in numerical simulation, and in Fig. 5(b) we compare the result with D varying from 2 to 30. We see that the result at $D = 5$ has correctly demonstrated the algebraic decay of the spin correlation function and almost converged to the result at $D = 30$. So we do not necessarily need a large internal dimension for the tensor network algorithm to uncover the algebraic decay associated with a spin liquid state. Keeping the same internal dimension at $D = 5$, we turn on J_1 (now a 2D model with $J_2 > J_1 > 0$), and find that long range spin correlation appears along the diagonal chains (see Fig. 5(a)), indicating that the spin order along this direction is very likely a real effect.

Although our numerical program can not distinguish the energy of the four degenerate states shown in Fig. 3(c,d) at the $J_2 > J_1$ side, it is very likely that the stripe

phase will emerge as the real ground state in practice because of its robustness to perturbation in the Hamiltonian. In real realization of the model Hamiltonian (1), the J_1 coupling along the horizontal and the vertical directions might be slightly different, or apart from the J_2 coupling on the checkerboard pattern, there might be small antiferromagnetic J_2 coupling along the other plaquettes. With any of these types of perturbation (which sound to be inevitable in practice), the energy of the Neel*-state will be lifted, and the stripe phase will emerge as the unique ground state of the system.

In summary we have used the iPEPS method, a type of tensor networks algorithms, to calculate the ground states of the frustrated anti-ferromagnetic J_1 - J_2 Heisenberg model on a checkerboard lattice. We construct the complete phase diagrams, indicating two first order phase transitions, first from a Neel state to a plaquette valence bond solid and then to a spin stripe phase. The calculation helps to clarify some of the previous debates on the phase diagram of this important model and provides a novel example for applications of the recently developed tensor network algorithms to frustrated systems.

We thank Subir Sachdev and Chao Shen for helpful discussions. This work was supported by the NBRPC (973 Program) 2011CBA00300 (2011CBA00302), the DARPA OLE program, the IARPA MUSIQC program, the ARO and the AFOSR MURI program.

-
- [1] P.Sindzingre, J.-B. Fouet, and C. Lhuillier, Phys. Rev. B **66**, 174424 (2002).
 - [2] O. A. Starykh, R.R.P. Singh, and G.C. Levine, Phys. Rev. Lett. **88**, 167203 (2002).
 - [3] O. A. Starykh, A. Furusaki, and L. Balents, Phys. Rev. B **72**, 094416 (2005).
 - [4] S. Moukouri, Phys. Rev. B **77**, 052408 (2008).
 - [5] W. Brenig and M. Grzeschik, Phys. Rev. B **69**, 064420 (2004).
 - [6] O. Tchernyshyov *et al.*, Phys. Rev. B **68**,144422 (2003).
 - [7] J. S. Bernier *et al.*, Phys. Rev. B **69**, 214427 (2004).
 - [8] G. Vidal, Phys. Rev. Lett. **93**, 040502 (2004); F. Verstraete, J. I. Cirac, cond-mat/0407066.
 - [9] J. Jordan *et al.*, Phys. Rev. Lett. **101**, 250602 (2008).
 - [10] B. Bauer, G. Vidal, and M. Troyer, J. Stat. Mech. P09006 (2009).
 - [11] V. Murg, F. Verstraete, and J. I. Cirac, Phys. Rev. B **79**, 195119 (2009).
 - [12] G. Evenbly, G. Vidal, Phys. Rev. Lett. **104**, 187203 (2010).
 - [13] A finite unit cell could suppress incommensurate spin orders, although such incommensurate orders do not sound to be a likely candidate for the ground state of the Hamiltonian (1).
 - [14] J. B. Fouet, M. Mambrini, P. Sindzingre, C. Lhuillier, Phys. Rev. B **67**, 054411 (2003).
 - [15] S. Sachedev and K. Park, Ann. Phys. (N.Y.) **298**, 58 (2002).